Organic Electronics 13 (2012) 992–998

Contents lists available at SciVerse ScienceDirect

Organic Electronics

journal homepage: www.elsevier.com/locate/orgel

Superficial fluoropolymer layers for efficient light-emitting diodes

Gianluca Latini [a,b], Li Wei Tan [a], Franco Cacialli [c], S. Ravi P. Silva [a,*]

[a] Nanoelectronics Center, Advanced Technology Institute, University of Surrey, Guildford, Surrey GU2 7XH, UK
[b] Center for Biomolecular Nanotechnologies@UNILE Istituto Italiano di Tecnologia, Via Barsanti, 73010 Arnesano (LE), Italy
[c] Department of Physics and Astronomy and London Center for Nanotechnology, University College London, Gower Street, WC1E 6BT London, UK

ARTICLE INFO

Article history:
Received 23 November 2011
Received in revised form 15 February 2012
Accepted 18 February 2012
Available online 9 March 2012

Keywords:
Polymer
Interlayer
OLED
Electrode
Fluoropolymer

ABSTRACT

Fluoropolymers are characterized by high chemical inertness and, when in solid state, by superficial dipoles due to the C–F bond where the charge density is strongly displaced. These two characteristics are exploited here for fine control of charge balance in organic light-emitting devices and for preventing electrochemical interaction between heterogeneous layers. The insertion of a thin layer of polytetrafluoroethylene, PTFE, at the interface between poly(ethylene dioxythiophene):poly(styrene sulfonic acid), PEDOT:PSS, and an electroluminescent polymer leads to improved device efficiency and longevity. The presence of the superficial dipole increases the effective work function of the anode and improves the charge balance which enhances the external quantum efficiency, EQE, of the devices by up to a factor of two without significant effects on the luminance levels. The insertion of the PTFE layer reduces the photoluminescence quenching at the PEDOT:PSS/polymer interface, however we show that the EQE enhancement is mainly due to a better confinement of minority carrier electrons in the active layer. The lifetime of the devices shows a remarkable increase correlated with the insertion of the PTFE layer. Such improvements are ascribed to the reduced electrochemical interaction between the electroluminescent polymer and PEDOT:PSS due to the chemically inert nature of PTFE. The PTFE acts as a chemical zipper of two heterogeneous media with the added functionality of control over the charge balance.

1. Introduction

The use of organic semiconductors for electronics has raised considerable interest based on their tunability of molecular properties and their potential for low-cost technology [1–3]. Organic light-emitting diodes (OLEDs), for example, have reached impressive performance, however device stability and longevity are still open issues that limit large-scale commercialization [4].

The light output efficacy of OLEDs is strongly dependent on the electrodes that inject and confine charges in the emitting layer controlling, then, the brightness and electroluminescence (EL) efficiency. In this context poly(ethylene dioxythiophene):poly(styrene sulfonic acid), PEDOT:PSS, has attracted enormous attention since it features suitable optical and electrical performance as a transparent electrode: high work function (WF) (4.5–5 eV), small electrical sheet resistance and high transmittance in the visible [5]. It has been shown that this blend vertically phase segregates and an insulating negatively-charged PSS-rich top layer (5–15 nm thick) is formed [6]. Such a layer blocks electrons enabling a reduction/cancellation of the energy barrier at the PEDOT:PSS/emissive layer interface thus assisting the hole injection [6–8]. This may further enhance electron injection, with an uncontrolled feedback mechanism dictated by the PEDOT:PSS/electron interface [9]. Despite its beneficial properties, PEDOT:PSS also suffers from many drawbacks: strongly acidic character (pH $\sim$ 1.7) [10], electromigration (of $PEDOT^+$) [11,12], and quenching of radiative emission [13,14]. In this article, we propose the use of a few nm-thick superficial fluoropolymer interlayer,

* Corresponding author.
E-mail address: s.silva@surrey.ac.uk (S. Ravi P. Silva).

1566-1199/$ - see front matter © 2012 Elsevier B.V. All rights reserved.
http://dx.doi.org/10.1016/j.orgel.2012.02.019

poly(tetrafluoroethylene) (PTFE, $(CF_2)_n$, Fig. S1), between PEDOT:PSS and an electroluminescent polymer. The exceptional chemical inertness of fluoropolymers like PTFE further enhance its functionality as an ideal 'zipper' of inhomogeneous layers [15]. Another important characteristic is that the fluorine atom, being the most electronegative element, displaces substantially the electronic charge distribution in its surrounding and the bond has ionic character which allows for large 'potential' steps in highly confined 2D geometries ideal for use in LED structures.

The major limiting factor for using PTFE in LEDs is its insulating nature (resistivity in the order of $\sim 10^8\,\Omega\,cm$) and its poor wetting properties that are a consequence of the superficial dipoles [16]. However, its chemical inertness is an extremely attractive property in organic electronic devices that are often subject to relatively fast degradation due to electrochemical interaction between inhomogeneous materials.

It has been reported that when a thin (~1 nm thickness) PTFE film is incorporated in OLEDs between ITO and the active layer, an enhancement of the hole injection occurs due to the PTFE rugged surface that induces localized charge-injection [17,18]. If the PTFE interlayer is thicker, then the insulating properties prevail reducing the hole injection. We recently employed ITO/PTFE electrodes in organic photovoltaic devices that revealed a ~200 mV increase of the open-circuit voltage when compared to ITO, suggesting the formation of an interfacial dipole [19].

We show that the insertion of PTFE in an OLED allows for the fine control of the charge balance by confining electrons into the emissive layer and by reducing hole injection. We also show that the PTFE interlayer is beneficial for the longevity of devices and assign this to reduced electrochemical interaction between the inhomogeneous components of the device. PTFE is insoluble in common solvents and inert to conventional chemical reagents. Alternative methods to solution process are preferred for PTFE coating as, for example, thermal or e-beam evaporation [17,18] or even friction-transfer techniques [20]. We study thermally-evaporated PTFE interlayers (nominal

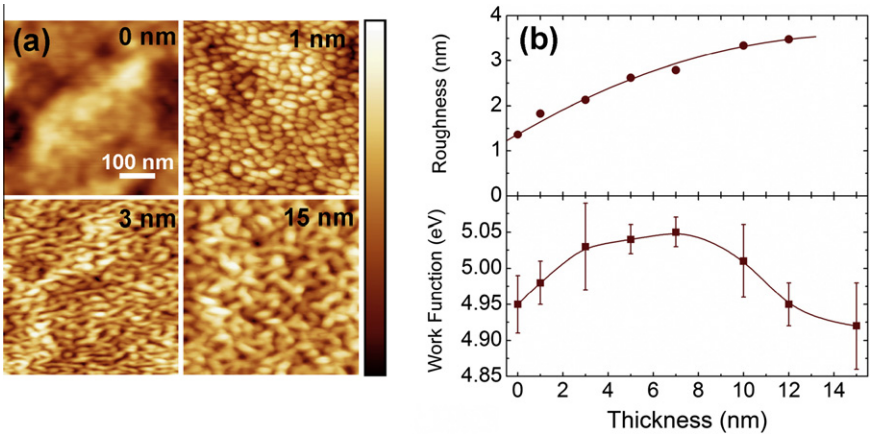

Fig. 1. (a) 500 × 500 nm^2 AFM height images of ITO/PEDOT:PSS and ITO/PEDOT:PSS/PTFE (x nm) films where x = 1, 3 and 15 nm and the vertical color scale bar is 9 nm, 10 nm, 13 nm and 17 nm, respectively. (b) (Top panel) RMS roughness of the samples as a function of the PTFE thickness measured over 2 images representing 5 × 5 μm^2 areas; (Bottom panel) work function measured with Kelvin probe of PEDOT:PSS/PTFE as a function of the PTFE thickness. The error bars are the standard deviation across 3 samples.

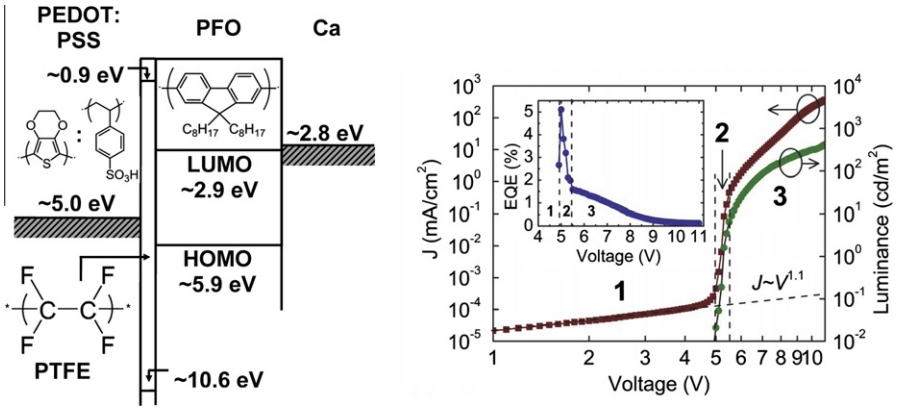

Fig. 2. (Left panel) Energy-level diagram for isolated materials of the OLED. The HOMO and LUMO of PFO, PTFE and the Fermi level positions of the electrodes are shown. The chemical structures of the polymeric materials are also shown. (Right panel) Representative current-light vs. voltage characteristic of a device incorporating a 7 nm PTFE interlayer. Three transport regimes are distinguished in the device characteristic. *Inset.* External quantum efficiency as a function of the voltage bias.

thickness ranging 1–15 nm) between PEDOT:PSS and poly(9,9-dioctylfluorene) (PFO) (Fig. 1). Despite the low wettability of PTFE, it was possible to spin coat polymer films on PEDOT:PSS/PTFE substrates and fabricate ITO/PEDOT:PSS/PTFE/PFO/Ca OLEDs (Fig. 2). The study of the current/luminance vs. voltage (ILV) characteristics of these devices show a modified charge balance that can be ascribed to dipole formation at the PEDOT:PSS/PTFE interface as corroborated by WF measurements [16].

So, PTFE allows for the effective control of the charge balance leading to improve efficiency, without reducing the brightness of the devices.

We also find that devices incorporating the PTFE interlayer present an extended device lifetime (up to ca. 4 times longer for the most efficient devices) indicating that PTFE acts as electrochemical barrier between the layers of the device.

2. Results and discussion

In Fig. 1 are reported representative Atomic Force Microscopy (AFM) images of ITO/PEDOT:PSS and ITO/PEDOT:PSS/PTFE. The morphology of PEDOT:PSS surface consists of a smooth topography with 200–300 nm-sized domains due to lateral phase separation of PEDOT and PSS [21]. When deposited in thin films (e.g., 1 nm thickness) on PEDOT:PSS, PTFE forms islands with a lateral size of ca. 10–30 nm. For thicker PTFE films (e.g., 3 nm) the islands coalesce and become elongated structures. When the PTFE thickness is further increased the lateral size of the features is larger and increases progressively. The root-mean-square roughness of the films is 1.36 ± 0.02 nm for PEDOT:PSS and progressively increases as a function of the PTFE thickness reaching 3.5 nm for 12 nm-thick PTFE films (Fig. 1b top panel).

The WF measured by Kelvin probe method (KP) for PEDOT:PSS was found to be 4.95 ± 0.04 eV in agreement with earlier reports (Fig. 1b bottom panel) [12,22]. When PTFE is deposited on top of PEDOT:PSS, the WF increases with thickness and reaches a maximum of 5.05 ± 0.02 eV for PEDOT:PSS/PTFE (7 nm) and then decreases to values comparable with that of bulk PEDOT:PSS.

The analysis of the characteristics of the ITO/PEDOT:PSS/PTFE/PFO/Ca/Al device (Fig. 2) show similar voltage dependence for all PTFE thicknesses studied including the reference device without PTFE (in Fig. S2 we report representative device characteristics for each PTFE thickness). We distinguish three regimes: (1) the linear current regime ($I \sim V^x$, $x = 1.1$) at low voltage; (2) the turn-on regime, with the sharp enhancement in current density of several orders, and, (3) the device operational regime. A space-charge-limited current model with a field-dependent mobility [23] can be used to describe the transport, which after switching, is bulk-limited [8] for the PTFE layers with thickness up to 10 nm. Above these values, the model fails to describe the characteristics.

Charge transport in PFO is typically hole-dominated and only poor electron transport has been observed [24]. However, work by van Woudenbergh [8], in the same device architecture as studied here, demonstrates that the initial current at low voltage (regime 1) is not dependent on the anode and can be attributed to electron dominance, with a linear dependence consistent with the formation of an ohmic contact at the Ca cathode. The injected electrons drift towards the anode interface where they are blocked and form a space-charge layer that assists hole injection, and the device turns on (regime 2) [7,8]. Since holes are more mobile than electrons, the hole population rapidly increases so to balance first, and then prevail on the electrons as it can be deduced from the sharp increase in the EQE and its subsequent decrease (inset in Fig. 2b). In regime 3 current and luminance curves are not as steep as in regime 2 and the device is fully on [9]. The EQE is decreasing with voltage reflecting a poorer charge balance (holes exceeding electrons more and more) and, possibly, current-induced radiative emission quenching, but not degradation as proved by the reproducibility of repeated IVL scans.

The EL turn-on voltage displayed little dependence upon the PTFE thickness apart from a measurable increase ($\sim$0.2–0.3 V) for the devices with PTFE interlayers thicker than 10 nm. In order to study the charge balance, we compare the EQE of the devices at the same current density, J (Fig. 3a). We select $J = 1$ mA/cm^2 (onset of EL turn-on) and $J = 10$ mA/cm^2 (device fully on). At 1 mA/cm^2 the device is very efficient, but the luminance quite low. At 10 mA/cm^2 the luminance is much higher and the device more stable. We observe that the EQE presents analogous trends for both these two current density regimes i.e., the EQE increases with the insertion of PTFE and is maximized for thickness ranging between 3 and 7 nm. In the case of $J = 1$ mA/cm^2, there is an enhancement by a factor 1.5 (from $\sim$0.8% to $\sim$1.2%), while for higher J the efficiency is approximately doubled (from $\sim$0.4% to $\sim$0.8%). Devices incorporating PTFE films thicker than 7 nm display a progressive reduction of the EQE with PTFE thickness.

The current below the turn-on voltage is electron-dominated, while above turn-on the device is essentially bipolar, and that holes are the majority carriers, so we analyze the current density for the series of devices for V_{bias} below (3 V – electron only) and above (6 V – hole dominated), the turn-on voltage (Fig. 3b). In contrast with what is observed for ITO/PTFE/emissive layer/cathode devices studied by Qiu et al. [17,18], no current injection enhancement is observed, even for the thinnest (i.e., 1 nm) PTFE layer and the current density decreases sharply with insertion of PTFE films in both regimes, However, while for the case of electrons ($V_{bias} = 3$ V) the J decreases by two decades, only one order of magnitude reduction is reported for at the hole-majority regime ($V_{bias} = 6$ V) suggesting that PTFE is more effective at blocking the electrons than at limiting hole injection.

The trend of luminance (Fig. 3c) reflects the product of the J and EQE, so it is essentially decreasing (as for J) with a relative maximum corresponding to the values of the PTFE thickness where the EQE is maximum, i.e., 3–7 nm. It is worth noting that in this range of thicknesses the luminance is comparable with the reference device without the PTFE interlayer.

In order to decouple the effect of the PTFE insertion on the charge balance from the photoluminescence (PL)

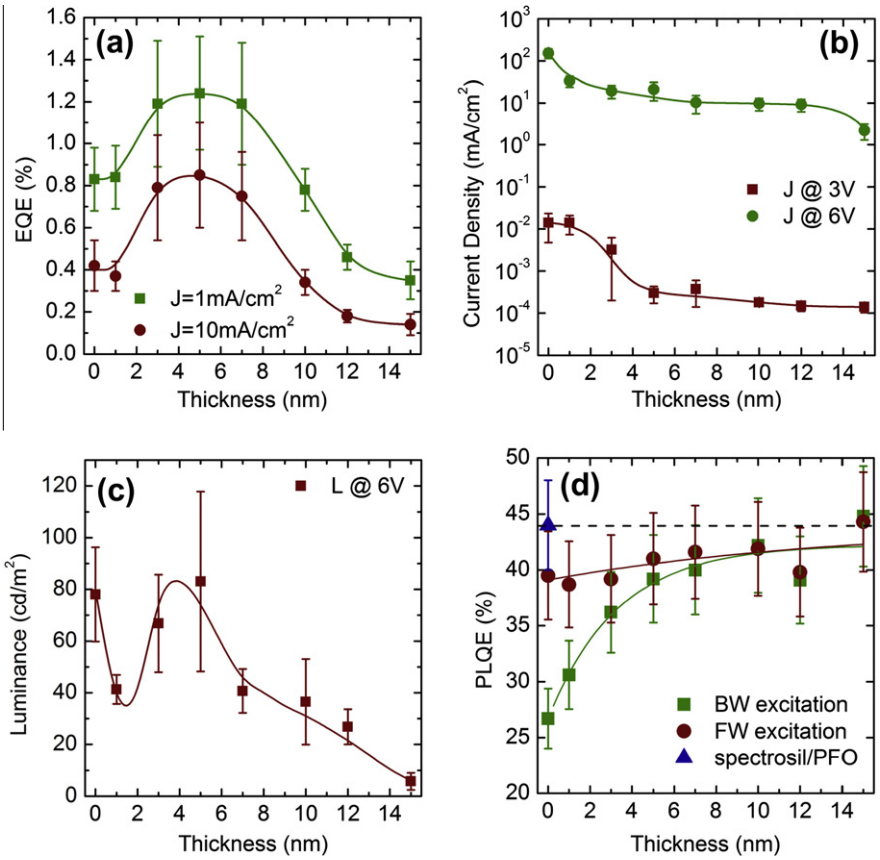

Fig. 3. (a) External quantum efficiency as measured for current density $J = 1$ mA/cm^2 (squares) and 10 mA/cm^2 (circles); (b) Current density below ($V_{bias} = 3$ V) and above ($V_{bias} = 6$ V) the turn-on voltage; (c) Luminance as measured at 6 V. (d) Values of the photoluminescence quantum efficiency of PFO when deposited on ITO/PEDOT:PSS, ITO/PEDOT:PSS/PTFE and spectrosil substrates. With squares are indicated the data obtained exciting the PFO from the ITO/PEDOT:PSS/PTFE side (backward, BW) while the circles are the data for the case in which the PFO is excited directly.

enhancement that is expected with the insertion of an insulator between PEDOT:PSS and the emissive layer [14], we measured the PL quantum efficiency (PLQE) of glass/ITO/PEDOT:PSS/PTFE/PFO samples with an integrating sphere. We carried out the experiments exciting the PFO from the glass/ITO/PEDOT:PSS side (backward excitation, BWE) and from the opposite side (forward excitation, FWE) (Fig. 3d). At the incidence angle used for the experiments (i.e., 45°), considering the absorption coefficient (ca. 2.3×10^5 cm^{-1} as we measured normalizing the absorption by the thickness of the films) at the excitation energy (3.3 eV), it can be estimated that ~50% of light is absorbed in the first ~20 nm of the polymer film. So, depending on which side the PFO is excited, it is possible probe the PLQE at the air/PFO or PEDOT:PSS/PTFE/PFO interface and, then, the effect of the PTFE layer. Measurements show a monotonous increase of the PLQE for both configurations and the efficiency asymptotically reaches the value measured for PFO deposited on spectrosil, i.e., 44%. However, while only a weak dependence upon PTFE thickness is observed for FWE measurements, the experiment exciting the polymer from the PEDOT:PSS side is more sensitive and PLQE almost doubles increasing from 27% to 44%.

The lifetime of the non-encapsulated devices, when driven at constant current density (100 mA/cm^2) in low vacuum (10^{-1}–10^{-2} mbar), is reported in Fig. 4a. Data show a remarkable increase of the longevity of the devices that clearly correlates with PTFE layer thickness. For the most efficient devices, 7 nm for example, we register an increase of a factor 4 (Fig. 4b). Since the experiment was carried out at constant current density, the value of the EL intensity directly reflects the EQE, so being more efficient, the device with the PTFE interlayer is also brighter. We observe that the EL for the device with PTFE, decreases progressively with time, whereas for the device without PTFE, the reduction of the EL, is followed, after a certain operating time, by an increase of the EL intensity.

Both types of devices become more and more resistive and the applied voltage necessary to sustain a constant current with the operating time increases linearly (Fig. 4c). Although, the insertion of the insulating PTFE layer requires an initial higher applied voltage, the voltage increase rate with time is lower for the devices incorporating the PTFE layer.

In Fig. 4d we report the study of the evolution of the EL spectra as a function of the operating time for devices with

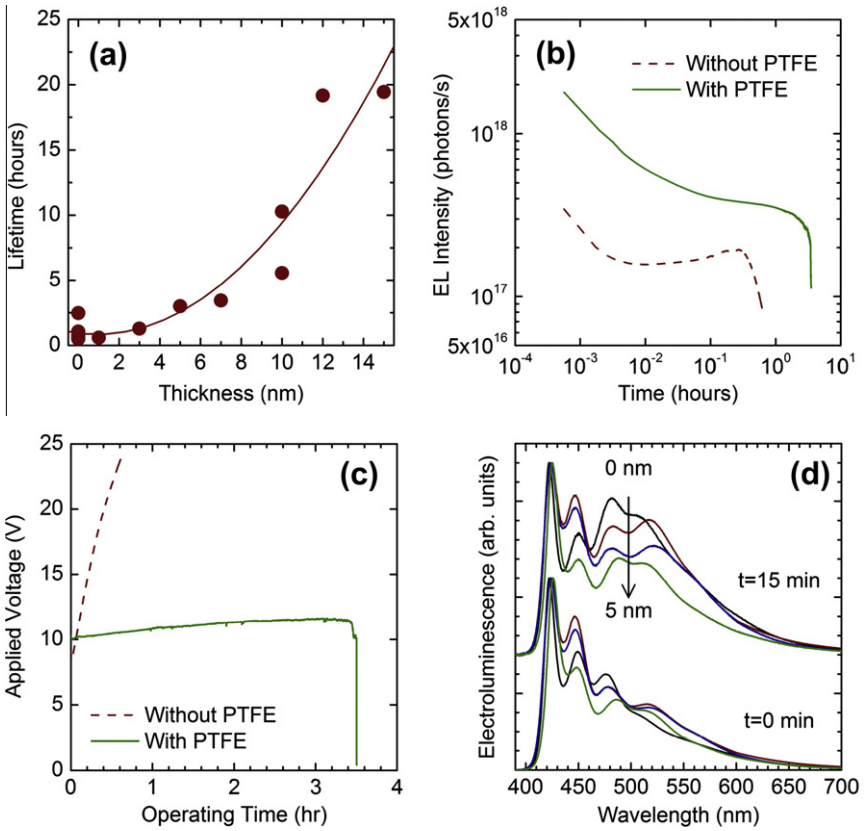

Fig. 4. Longevity study of non-encapsulated ITO/PEDOT:PSS/PTFE/PFO/Ca/Al devices carried out at constant current density (100 mA/cm^2) in low vacuum (10^{-1}–10^{-2} mbar). The lifetime of the device is defined as the time at which the EL intensity is equal to 10% of its initial value. (a) Lifetime of the devices as a function of the PTFE interlayer thickness. (b) Electroluminescence intensity and (c) voltage bias as function of time of the devices with 7 nm PTFE interlayer and without. (d) Electroluminescence spectra normalized to the 0–0 peak (solid lines) of ITO/PEDOT:PSS/PTFE(x nm)/PFO/Ca/Al driven at constant current (50 mA/cm^2). Spectra were recorded after driving the devices for 0 (bottom) and 15 min (top) where x = 0 (black), 1 (red), 3 (blue) and 5 nm (green). (For interpretation of the references to color in this figure legend, the reader is referred to the web version of this article.)

PTFE interlayers 1, 3 and 5 nm. EL spectra display analogous vibronic structure to the PL (see Fig. S2), however they differ in the region between 480 and 520 nm where a broad component, referred in literature as "green band" (g-band) appears [25–27]. The latter becomes more intense with the device operating time and it is typically associated with the degradation of the device (see also Fig. S3). While the intensity of such does not differ significantly for the spectra at t = 0, differences are observed after 15 min and clearly the g-band is more intense for thinner PTFE interlayers.

Our results do not show hole-injection enhancement as reported and predicted by Wu et al. [17,18]. Indeed their proposed model predicts hole-injection enhancement only in presence of isolated rough grains. They reported PTFE forming rough surfaces on ITO and islands coalescing at thicknesses of ~15 nm [17,18] while, we observe that PTFE on PEDOT:PSS begin to coalesce at only ~3 nm [18].

The measured change of the effective WF (Fig. 1b bottom panel) does suggest the presence of a dipole. However, it has to be noted that the effective WF is measurable with the KP only for thin layers, while for thicker films the experiment is not sensitive to the substrate anymore and does not provide a measurement of the vacuum level shift at the interface [28]. So, although direct confirmation with photoelectron spectroscopy would be required, the increase of the effective WF for thin PTFE layers can be assigned to a dipole effect. Indeed, such an effect is highly plausible, since it would agree with the presence of superficial dipoles as expected for fluoropolymers [16]. The increase of the effective WF, with thickness may be related to a more ordered molecular nanostructure in thicker films that generates a more intense superficial dipole.

According to these considerations and combined with its low electron affinity ($LUMO_{PTFE} \approx 0.6$ eV) [29], it can be postulated that the PTFE acts as an electron-blocking layer. On the other hand, the holes experience a large energy barrier at the PTFE/PFO interface ($HOMO_{PTFE} \approx$ 10.6 eV) [29] and hole injection is expected to be strongly reduced by the insertion of the PTFE layer.

When PTFE interlayer is incorporated in the devices, such dipoles play a role similar to the negatively-charged PSS-rich layer in PEDOT:PSS. So, the device still presents the three regimes in which an electron-only regime is followed by a sharp transition where the holes start to be injected and the on-state. In the latter state, when increasing

the PTFE thickness, the current density decreases, but values of the luminance are preserved for the most efficient devices (5–7 nm PTFE thick layer). Indeed, luminance is governed by the minority carriers so this agrees with the hypothesis in which the electrons are efficiently kept confined in the PFO layer.

The improved EQE, for intermediate thicknesses, has to be decoupled by the effect due to the increase of the PL quantum efficiency (Fig. 3d). First we notice that PLQE only increases from 27% to ca. 40% for BWE while EQE increases even by a factor two for 3–7 nm-thick PTFE. Also, since the device is hole-dominated at operational voltages, the recombination zone is expected to be away from the anode and then relatively insensitive to changes of the PLQE due to insertion of the PTFE interlayer at the PEDOT:PSS/PFO interface. So, we conclude that the EQE enhancement cannot be assigned exclusively to the prevented PL quenching at PEDOT:PSS interface, but that a modified charge balance is likely to play the most important role, in agreement with the presence of superficial dipoles at the PTFE surface as suggested by the ILV analysis and WF measurements.

The direct correlation between the increase in lifetime of the devices with the insertion of the PTFE layer (Fig. 4) indicates that the PTFE interlayer is able to significantly slow down the degradation processes that are related to the PEDOT:PSS/PFO interface. For example, Kim et al. [30] identified one of the mechanisms that leads to a more resistive character of the PEDOT:PSS/emissive polymer interface. This is due to local de-doping of the PEDOT:PSS that occurs in correspondence of pin holes at the cathode. The slower evolution of the resistivity for the devices incorporating PTFE (Fig. 4c) suggests that the PTFE layer protects the PEDOT:PSS and prevent such de-doping process. The fact that, for the device without PTFE interlayer, the EL intensity (and efficiency) does not decrease monotonically, but, after a time increases, indicates a charge balance modification associated to the degradation of the electrode associated to the majority carriers (in this case the PDOT:PSS/PTFE). Such a change in the EL time evolution is not observed for the device with PTFE, suggesting a prevented aging of PEDOT:PSS, protected by the PTFE itself.

The PL and EL emission of PFO is often characterized by the occurrence of an emission at low energy, so-called *g*-band, that differs from the pure intra-chain fluorene emission [25,26]. This "spurious" feature is correlated with degradation of the device and it is undesirable because it significantly quenches the radiative efficiency and affects the color purity. The spectral location of the *g*-band is usually found peaked at about 535 nm, however an additional spectral feature has been found in EL, at shorter wavelength (i.e., between 475 and 510 nm) and is correlated to the presence of Ca electrodes that catalyzes oxidative processes [25,27]. Furthermore, such spectral feature is more intense when the recombination zone is located closer to the more defective region near the Ca cathodes.

We attribute the occurrence of the green emission in our devices to the latter phenomenon since its spectral region better fits than for the typical fluorenone emission. This also agrees with the modified charge balance induced by the PTFE insertion in favor of electrons since, in this case, the recombination zone would shift away from the defective region in the vicinity of the Ca cathode. Thus, a less intense green emission follows.

3. Conclusions

In conclusion, we show that despite its low wettability, when a few nm-thick film of PTFE is deposited as interlayer on PEDOT:PSS it still allows fabrication of solution-processed polymer-based OLEDs. We measure an increase of the effective WF of PEDOT:PSS/PTFE when compared to PEDOT:PSS only. The hypothesis for the formation of interfacial dipoles is confirmed by the study of the characteristics of OLEDs that show improved electron confinement with the PTFE interlayer. The analysis of device characteristics shows that the PTFE layer is capable of controlling the charge balance, which maximizes the efficiency of the OLED without altering the light output. Measurements of the PLQE at grazing angles confirm that insertion of PTFE is beneficial to prevent the PL quenching at the anode/polymer interface. However, the enhancement of the EQE is due mainly to the improved charge balance rather than to the reduced electrode-induced PL quenching.

Devices also report a dramatic improvement of the longevity indicating that the interlayer slows down aging processes like electrochemical interaction and ion diffusion.

The improved efficiency and stability with the insertion of nm-thick chemically-inert PTFE layers is a remarkable result that could be further improved by using other types of fluoropolymers or modifying the deposition techniques in order to enhance the intensity of the dipole.

4. Experimental details

ITO/PEDOT:PSS/PTFE/PFO/Ca/Al OLEDs were fabricated using ITO substrates that were preliminarily solvent cleaned (10 min ultrasonic bath in acetone and isopropanol) and then treated with oxygen-plasma [31]. Thin films (60–80 nm) of PEDOT:PSS (Baytron P AI 4083) were deposited in air by spin coating and then annealed at 120 °C in nitrogen. PEDOT:PSS films were then transferred in air to an evaporation chamber where PTFE sheets (density = 2.17 ± 0.02 g/cm^3) thermally evaporated at 10^{-6} mbar (evaporation rate = 0.1 nm/s), and transferred (in air) to a glove box where PFO films (thickness ~90–110 nm) were deposited in nitrogen by spin coating *p*-xylene solutions (2% by weight). No annealing treatment was applied to the PFO films. PFO-end capped with dimethyl-phenyl was purchased by American Dye Source (ADS129BE, Mw = 48,800). Calcium(30 nm)/Aluminium(150 nm) electrodes were thermally evaporated at 10^{-6} mbar on the polymer films. The thickness of the polymer films (90–110 nm) was measured using a Dektak profilometer. Non encapsulated devices were characterized in low vacuum (ca. 10^{-1}–10^{-2} mbar) after being transferred, under nitrogen, from the glove-box used for the cathode deposition. A source meter (Keithley 2400) was used to drive the devices to measure the current and light-vs.-voltage characteristics and for lifetime measurements. The EL output was measured with a calibrated silicon photodiode

[12]. The work function, φ, was measured, in air, by Kelvin probe measurement of the contact potential difference (CPD) [28]. The work function was calculated by referencing the CPD to the WF of highly oriented pyrolytic graphite, ϕ_{HOPG} = 4.475 eV [32]. The error bars are the standard deviation across 3 samples fabricated in different evaporations. The measurements, per each sample, were repeated in order to monitor the reproducibility of the measurements.

PLQE was obtained with the method of the integrating sphere. The PL and EL spectra were collected with an Andor Shamrock spectrograph (spectral resolution ~1 nm) coupled with a charge coupled device, CCD. The PL measurements were conducted exciting the samples with a diode laser (E_{exc} = 3.3 eV). For the photoluminescence efficiency an incidence angle of 45° was used in order to enhance the sensitivity of the measurement to the PEDOT:PSS/PTFE/PFO interface when PFO was excited from the substrate side (backwards excitation) in contrast with excitation from the PFO side (forward).

The surface and film morphology was studied by atomic force microscope (Veeco DimensionTM 3100 Controller). Topography and phase images were simultaneously obtained using n^+-silicon cantilever supplied by Nanosensors with the resonance frequency 255 kHz and a force constant of 20 N/m. The surface flatness was characterized by its root-mean-squared roughness, R_{RMS}, of $N \times N$ pixels images $R_{RMS} = \sqrt{\frac{1}{N^2-1}\sum_{m,n=1}^{N}(h_{m,n} - \langle h \rangle)}$where $h_{m,n}$ is the height value of the pixel (m,n) and $\langle h \rangle$ is the mean height of the pixels calculated from $N \times N$ values. R_{RMS} was determined from 5×5 μm^2 areas.

Acknowledgements

The authors thank the Carbon Trust and the EPSRC for sponsoring the research via a Portfolio Partnership Award to the University of Surrey. Work at UCL was supported by the EC (EU-contract: MRTN-CT-2006-036040), the EPSRC, the European Science Foundation EUROCORES Program SONS with supplementary funds from EPSRC, and the EC Sixth Framework Program, under contract N. ERAS-CT-2003-980409.

Appendix A. Supplementary data

Supplementary data associated with this article can be found, in the online version, at doi:10.1016/j.orgel.2012.02.019.

References

[1] J.H. Burroughes, D.D.C. Bradley, A.R. Brown, R.N. Marks, K. Mackay, R.H. Friend, P.L. Burns, A.B. Holmes, Nature 347 (1990) 539.
[2] N.S. Sariciftci, L. Smilowitz, A.J. Heeger, F. Wudl, Science 258 (1992) 1474.
[3] A.R. Brown, A. Pomp, C.M. Hart, D.M. de Leeuw, Science 270 (1995) 972.
[4] S. Reineke, F. Lindner, G. Schwartz, N. Seidler, K. Walzer, B. Lussem, K. Leo, Nature 459 (2009) 234.
[5] L. Groenendaal, F. Jonas, D. Freitag, H. Pielartzik, J.R. Reynolds, Adv. Mater. 12 (2000) 481.
[6] P.C. Jukes, S.J. Martin, A.M. Higgins, M. Geoghegan, R.A.L. Jones, S. Langridge, A. Wehrum, S. Kirchmeyer, Adv. Mater. 16 (2004) 807.
[7] K. Murata, S. Cina, N.C. Greenham, Appl. Phys. Lett. 79 (2001) 1193.
[8] T. van Woudenbergh, J. Wildeman, P.W.M. Blom, J.J.A.M. Bastiaansen, B.M.W. Langeveld-Vos, Adv. Funct. Mater. 14 (2004) 677.
[9] T.M. Brown, F. Cacialli, J. Polym. Sci. Part B: Polym. Phys. 41 (2003) 2649.
[10] H.C. Starck, Overview CLEVIOS™ general properties (2009) 3430. Available from: <http://www.clevios.com/index.php>.
[11] R.-Q. Png, P.-J. Chia, S. Sivaramakrishnan, L.-Y. Wong, M. Zhou, L.-L. Chua, P.K.H. Ho, Appl. Phys. Lett. 91 (2007) 013511.
[12] G. Winroth, G. Latini, D. Credgington, L.-Y. Wong, L.-L. Chua, P.K.-H. Ho, F. Cacialli, Appl. Phys. Lett. 92 (2008) 103308.
[13] J. Morgado, R.H. Friend, F. Cacialli, Appl. Phys. Lett. 80 (2002) 2436.
[14] J.-S. Kim, R.H. Friend, I. Grizzi, J.H. Burroughes, Appl. Phys. Lett. 87 (2005) 023506.
[15] R.R. Thomas, in: G.G. Hougham, P.E. Cassidy, K. Johns, T. Davidson (Eds.), Fluoropolymers, vol. 2, Kluwer Academic Publishers, 1999, p. 47.
[16] S. Lee, J.-S. Park, T.R. Lee, Langmuir 24 (2008) 4817.
[17] Y. Gao, L. Wang, D. Zhang, L. Duan, G. Dong, Y. Qiu, Appl. Phys. Lett. 82 (2003) 155.
[18] Z. Wu, L. Wang, H. Wang, Y. Gao, Y. Qiu, Phys. Rev. B 74 (2006) 165307.
[19] B. Kang, L.W. Tan, S.R.P. Silva, Appl. Phys. Lett. 93 (2008) 133302.
[20] J.C. Wittmann, P. Smith, Nature 352 (1991) 414.
[21] S. Timpanaro, M. Kemerink, F.J. Touwslager, M.M. De Kok, S. Schrader, Chem. Phys. Lett. 394 (2004) 339.
[22] N. Koch, A. Elschner, J.P. Rabe, R.L. Johnson, Adv. Mater. 17 (2005) 330.
[23] G.G. Malliaras, J.R. Salem, P.J. Brock, C. Scott, Phys. Rev. B 58 (1998) R13411.
[24] T. Kreouzis, D. Poplavskyy, S.M. Tuladhar, M. Campoy-Quiles, J. Nelson, A.J. Campbell, D.D.C. Bradley, Phys. Rev. B 73 (2006) 235201.
[25] S. Gamerith, C. Gadermaier, U. Scherf, E.J.W. List, in: W. Brütting (Ed.), Physics of Organic Semiconductors, Wiley-VCH, 2005, p. 153.
[26] S.-F. Lim, R.H. Friend, I.D. Rees, J. Li, Y. Ma, K. Robinson, A.B. Holmes, E. Hennebicq, D. Beljonne, F. Cacialli, Adv. Funct. Mater. 15 (2005) 981.
[27] X. Gong, P.K. Iyer, D. Moses, G.C. Bazan, A.J. Heeger, S.S. Xiao, Adv. Funct. Mater. 13 (2003) 325.
[28] H. Ishii, N. Hayashi, E. Ito, Y. Washizu, K. Sugi, Y. Kimura, M. Niwano, Y. Ouchi, K. Seki, in: W. Brütting (Ed.), Physics of Organic Semiconductors, Wiley-VCH, 2005, p. 69.
[29] K. Seki, H. Tanaka, T. Ohta, Y. Aoki, A. Imamura, H. Fujimoto, H. Yamamoto, H. Inokuchi, Physica Scripta 41 (1990) 167.
[30] J.-S. Kim, P.K.H. Ho, C.E. Murphy, N. Baynes, R.H. Friend, Adv. Mater. 14 (2002) 206.
[31] J.S. Kim, F. Cacialli, M. Granstrom, R.H. Friend, N. Johansson, W.R. Salaneck, R. Daik, W.J. Feast, Synth. Met. 101 (1999) 111.
[32] G. Latini, M. Wykes, R. Schlapak, S. Howorka, F. Cacialli, Appl. Phys. Lett. 92 (2008) 013511.